Attosecond Time-Resolved Imaging of Molecular Structure by Photoelectron Holography

Xue-Bin Bian and André D. Bandrauk*

Département de Chimie, Université de Sherbrooke, Sherbrooke, Quebéc J1K 2R1, Canada

(Received 3 March 2012; published 27 June 2012)

Dynamic imaging of the molecular structure of H_2^+ is investigated by attosecond photoelectron holography. The interference between direct (reference) and backward rescattered (signal) photoelectrons in attosecond photoelectron holography reveals the birth time of both channels and the spatial information of molecular structure. This is confirmed by simulations with a semiclassical model and numerical solutions of the corresponding time-dependent Schrödinger equation, suggesting an attosecond time-resolved way of imaging molecular structure obtained from laser induced rescattering of ionized electrons. It is shown that both short and long rescattered electron trajectories can be imaged from the momentum distribution.

DOI: 10.1103/PhysRevLett.108.263003 PACS numbers: 32.80.Wr, 33.60.+q, 61.05.jp

Holography was invented in 1947 by Gabor [1]. Its central idea is to record the interference between a signal and a reference wave and to reconstruct the objects. Recently, Huismans *et al.* [2] reported an experimental photoelectron holographic structure by exposing metastable Xe in a mid-infrared free electron laser. This photoelectron holography (PH) [2,3] in above-threshold ionization (ATI) is different from optical holography. The reference and signal waves in PH produced by the laser fields come from the same object, but with different transverse momentum [2,4]. It is based on a laser-induced recollision model [5–8] of strong field physics. The electron liberated by a linearly polarized laser field with initial nonzero transverse momentum directly drifts to the detectors (reference). The free electron with initial zero or very small transverse momentum may be rescattered by the core, which then drifts to the detectors (signal). These two channels with the same final momentum will interfere with each other and record the attosecond subcycle ionization dynamics [2,4]. Due to the smaller atomic scattering cross sections, a "forklike" structure in PH recognized by Huismans *et al.* [2] is a kind of forward rescattering holography [4]. To our knowledge, the backward rescattering holography in ATI has not been reported. In this Letter, we investigate the time-resolved attosecond photoelectron holography (APH) of H_2^+ in MATI (molecular above-threshold ionization). For molecular ions with multiple centers and coulomb focusing effects, the rescattering cross sections are larger compared to atoms. As illustrated in Fig. 1, we identify two kinds of backward rescattering APH, corresponding to the "long" and "short" trajectories in the recollision model [5–7]. The backward rescattering APH can be used for dynamic imaging of molecular structure [9,10] and detecting electron motion in molecules [11] on attosecond time scale.

The semiclassical recollision model [5,6] has been proven to be successful in interpreting forward rescattering PH [2,4]. It can be used to describe such processes by a simple physical picture. We use next this model to predict the holographic structure in MATI of H_2^+. In the tunneling ionization regime, we assume the rescattered photoelectrons are first released with zero transverse velocity. When the laser field changes direction, the electrons are driven back and backward rescattered by the core because of the large rescattering cross sections. Since the kinetic energy of the electrons before rescattering can be as large as $3.17U_p$ where $U_p = E^2/4\omega^2$ (a.u.) is the ponderomotive energy, the corresponding de Broglie wavelength $\lambda_e = 2\pi/p$ may be comparable to or even smaller than the molecular internuclear distance R. We call this trajectory a signal wave, which can be used to explore molecular structure. The electrons in this channel obtain their transverse momentum during the rescattering process. For the direct photoelectrons, we assume they obtain their transverse momentum during the tunneling ionization process.

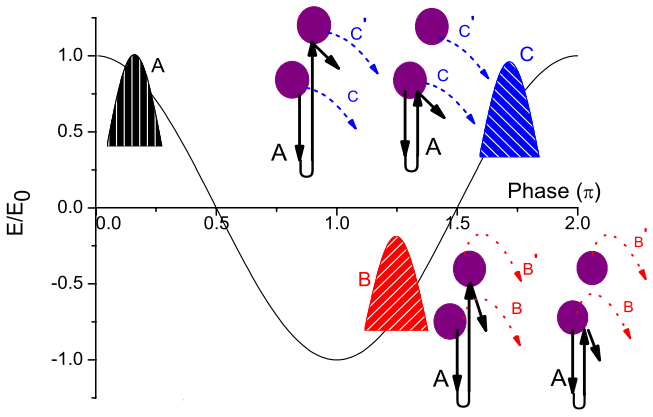

FIG. 1 (color online). Schematic illustration of interference trajectories in APH of H_2^+. A is the rescattering channel, its short and long trajectories will interfere with the direct ionization channels of B and C, respectively. Introducing multicenter molecular structure, channel A may be rescattered by the parent core or its neighboring core. Channels B (B') and C (C') may come from different centers.

In linearly polarized laser fields, due to the transverse displacement, such electrons will not collide with the core again. We call this trajectory the reference wave. When the reference and signal electrons reach the detector with the same momentum, the photoelectron momentum distribution spectra will record the interference structure of the holography. As suggested by the semiclassical model in Fig. 1, the rescattering signal channel A may have short and long trajectories with the same rescattering momentum, and interfere with reference electrons B and C from different subcycles will occur. To explore these novel interference structures, we next briefly introduce the semiclassical model to deduce the phase difference between the above trajectories.

We adopt the recollision three-step semiclassical model [5,6] and summarize the following conditions for APH interference: (i) The signal electron is born at initial distance $z_0 = I_p/E_0$ (atomic units, a.u., $\hbar = m_e = e = 1$ are used throughout.) from the core by tunneling ionization near the peak of the pulse. As proposed by Busuladžić *et al.* [12], there are up to six possible contributions leading to the same final momentum state. However, APH is restricted to energies around $2U_p$, which is determined by the maximum energy in the reference channel. We assume the initial signal and reference electrons are not spatially separated wave packets [12,13] because the internuclear distance is rather small ($R = 2$ a.u.), and the electronic de Broglie wavelength λ_e is larger than R. After ionization, we neglect the influence of the Coulomb potential due to large initial z_0 and α (where $\alpha = E_0/\omega^2$ is the oscillation amplitude of a free electron in the laser field) for the laser parameters used in present Letter. When the electron comes back to the cores, it has higher energy, and it is elastically scattered by the two cores. (ii) The initial velocity of the signal electron is $v_\parallel^{\text{signal}} = v_\perp^{\text{signal}} = 0$, while the initial velocity of the reference electron is $v_\parallel^{\text{ref}} = 0$, $v_\perp^{\text{ref}} \neq 0$. The signal electrons get their transverse momentum during rescattering by the cores, while the reference electrons obtain their transverse momentum initially during ionization. Then the momentum in the transverse direction is conserved. (iii) After rescattering, the velocity of the signal electron is the same as that of the reference electron. This is a condition for stable interference in momentum space. (iv) We neglect multiple rescattering of the signal electron by the cores.

For the laser field polarized along the z direction, the motion of electrons along the perpendicular direction is constant in the laser field. The molecular axis has an angle β with the z direction of the field polarization. In the following, we only consider the motion of electrons along the z direction. If the electron is ionized at an arbitrary phase φ of the electric field $E(t) = E_0\cos(\omega t + \varphi)$, the velocity and the position of the electron can be obtained from a classical model [14,15]:

$$\begin{aligned} v(t,\varphi) &= \int_0^t -E(t')dt' = -\frac{E_0}{\omega}[\sin(\omega t + \varphi) - \sin(\varphi)], \\ z(t,\varphi) &= \int_0^t v(t')dt' \\ &= \frac{E_0}{\omega^2}[\cos(\omega t + \varphi) - \cos(\varphi) + \omega\sin(\varphi)t] - z_0. \end{aligned} \tag{1}$$

When the electron is driven back to the core after a travel time t_c, $z(t_c, \varphi) = 0$, we obtain a relation between t_c and φ as:

$$\cos(\omega t_c + \varphi) - \cos(\varphi) + \omega\sin(\varphi)t_c = \gamma^2/2, \tag{2}$$

where $\gamma = \sqrt{2I_p}\omega/E_0$ is the Keldysh parameter [5,6].

Next, we assume that the electron is elastically backward rescattered by the core at an angle θ_c, $\theta_c \in [90°, 270°]$. After this process, the velocity in the perpendicular direction is constant: $v_\perp = v(t_c, \varphi)\sin(\theta_c)$. The final velocity along z direction is then obtained as:

$$\begin{aligned} v_\parallel(t) &= \int_{t_c}^t E(t')dt' \\ &= -\frac{E_0}{\omega}[\sin(\omega t + \varphi) - \sin(\omega t_c + \varphi)] \\ &\quad + v(t_c, \varphi)\cos(\theta_c). \end{aligned}$$

After taking into account that the vector potential $\mathbf{A}(t) = 0$ at the end of the pulse, the measured momentum by the detectors outside the field is:

$$P_\parallel = \frac{E_0}{\omega}\sin(\omega t_c + \varphi) + v(t_c, \varphi)\cos(\theta_c). \tag{3}$$

For the reference electron, under the interference condition, its ionization phase φ' and the traveling time t^r in the laser field satisfy the condition: $\varphi + \omega t_c = \varphi' + \omega t^r$. In addition, the parallel and transverse velocities are $v_\parallel(t^r, \varphi') = v(t_c, \varphi)\cos(\theta_c)$, $v_\perp = v(t_c, \varphi)\sin(\theta_c)$.

From the above, we obtain the phase difference between the signal and the reference electron as:

$$\begin{aligned} \Delta\Phi = &\int_0^{t_c} \frac{v^2(t', \varphi)}{2}dt' - \int_0^{t^r} \frac{v^2(t', \varphi')}{2}dt' - \frac{v_\perp^2 t^r}{2} \\ &- I_p\frac{(\varphi - \varphi')}{\omega}. \end{aligned} \tag{4}$$

If the electron is rescattered by the neighboring core, it will have an additional phase difference:

$$\Delta\Phi' = v(t_c, \varphi)R[\cos\beta - \cos(\beta + \theta_c)]. \tag{5}$$

We next confirm this model numerically by using a method [4] in 3D for solving the time-dependent Schrödinger equation (TDSE) in spherical coordinates [16] in the velocity gauge for static nuclei at fixed R. The 3D electronic Hamiltonian in a.u. for this static model is

$$H = \mathbf{p}^2/2 - 1/(\mathbf{r} - \mathbf{R}) - 1/(\mathbf{r} + \mathbf{R}) + \mathbf{A}(t)\cdot\mathbf{p}. \tag{6}$$

The wave function is expanded by B splines as $\Psi(r, \xi, \phi, t) = \Sigma_{i,j,m} C^{i,j,m}(t) B_i(r)(1 - \xi^2)^{(|m|)/2} B_j(\xi) \times [\exp(im\phi)/\sqrt{2\pi}]$, with $\xi = \cos\theta$. In our calculation, the number of B splines is 1200 in the radial direction with boundary $r_{\max} = 800$ a.u., and the number of B splines is 24 in the angular ξ direction. The magnetic quantum number of m is truncated at $M\,\max = 23$. The resulting order of the Hamiltonian matrix is 1 353 600. The initial state is the ground $1s\sigma_g$ state. The time evolution propagation used is the Arnoldi-Lanczos method [4]. The time step is $\Delta t = 0.01$ a.u., and a $\cos^{1/8}$ mask function is used to absorb the reflection from the boundary.

A long-wavelength laser field is not a necessary condition to observe APH [17]. Short wavelengths reduce the recollision time so that nuclear motion can be neglected. The wavelength of the laser field used in our simulation is $\lambda = 532$ nm ($\omega = 0.085$ a.u., $T_0 \approx 1.8$ fs), and the laser intensity is $I = 1.5 \times 10^{15}$ W/cm^2. The vector potential of the pulse is given by $\mathbf{A}(t) = \frac{E_0}{\omega} \sin^2(\frac{\pi t}{T}) \sin(\omega t)\mathbf{e_z}$, ensuring the total electric area of the field $\mathbf{E}(t) = -\frac{\partial \mathbf{A}}{\partial t}$ is zero. The total duration T of the laser field in TDSE is 5 cycles (9 fs). The vibrational period T_ν of H_2^+ is around 15 fs ($\omega_\nu \approx 2000$ cm^{-1}). $T < T_\nu$, and the recollision time $T_c \approx \frac{2}{3} T_0 \ll T_\nu$. So the fixed nuclei approximation is reasonable at 532 nm. The photoelectron angular distribution (PAD) by semiclassical predictions and TDSE simulations for perpendicular orientation (the molecular axis is along the x direction) and parallel orientation (the molecular axis is along the z direction) are presented in Figs. 2 and 3, respectively.

As illustrated in Fig. 1, the interference between channels A and B corresponds to short-trajectory rescattered electrons interfering with direct electrons. The dispersion of the rescattered wave packet is relatively small due to Coulomb focusing; as a result, this interference channel will dominate in the APH. As discussed above, the electron may also be rescattered by the neighboring ion. We present both of the PAD predicted by the semiclassical model in Fig. 2(a) (due to symmetry, we only show a quarter of the whole momentum space). For perpendicular orientation, i.e., x direction, the number of interference stripes with $P_z \in [-2, 0.5]$ a.u. predicted by the semiclassical model is 7, agree well with the TDSE results presented in Fig. 2(c). The interference maximum around $P_z = -2.5$ a.u. predicted by the semiclassical model is narrow, but it is still distinguishable in the TDSE. From $P_z = -0.5$ to -2.5 a.u., another obvious feature predicted by the semiclassical model is that the width of the stripes and the space between the stripes become larger, which agrees well with the TDSE results. However, the interference in the long rescattering trajectory is difficult to be observed in TDSE. The difficulty comes from two effects. One is due to the dispersion of the wave packet in the long trajectory, whose travel time $t > \frac{2}{3} T_0$. Consequently, the signal is weak. The other reason is from the mixing of interference stripes by the rescattering from

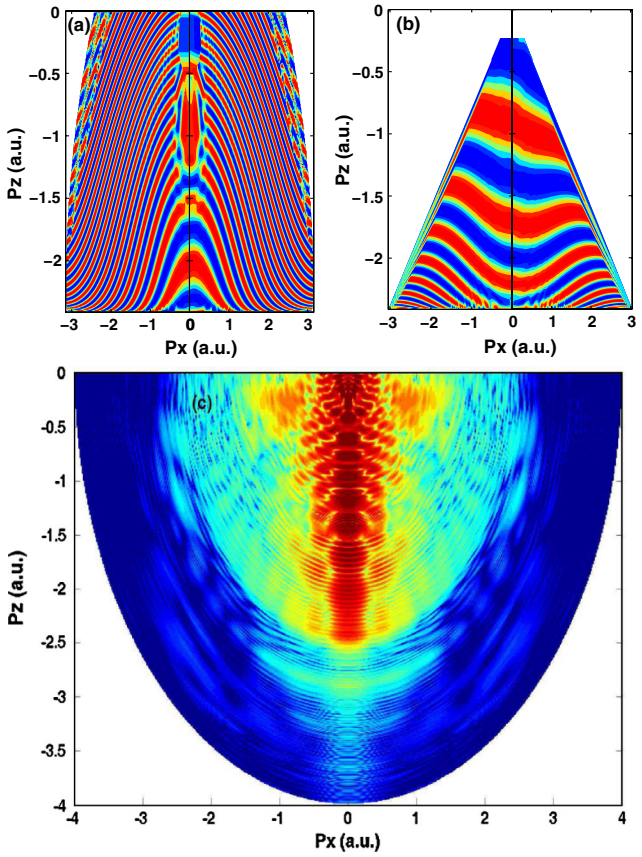

FIG. 2 (color online). Photoelectron angular momentum distribution of H_2^+ from the semiclassical model [(a) and (b)] and TDSE (c). (a) represents the short trajectory, while (b) stands for the long trajectory. The initial state is the ground $1s\sigma_g$ state. The internuclear distance $R = 2$ a.u. The laser intensity is $I = 1.5 \times 10^{15}$ W/cm^2, wavelength is 532 nm ($T_0 = 1.8$ fs). The molecular axis is along x axis, perpendicular to the laser polarization direction z. In (a) and (b), the left and right panels correspond to the photoelectron rescattered by the parent or the neighboring ions, respectively. In (c), the color is plotted on the logarithmic scale.

different centers. In the perpendicular orientation, Eq. (5) reduces to $\Delta\Phi' = v(t_c, \varphi) R \sin\theta_c = v_x R$. As illustrated in Fig. 2(b), the interference stripes are distorted with larger transverse momentum. The interference minimum from rescattering by one center may be overlapped by a maximum rescattering by the neighboring center. As a result, the long channel is not well resolved in the PAD by the TDSE.

For parallel orientation, i.e., z direction, Eq. (5) reduces to $\Delta\Phi' = v(t_c, \varphi) R(1 - \cos\theta_c)$. This additional phase has an influence on the interference stripes with larger rescattering momentum and smaller transverse momentum. As illustrated in Fig. 3(a) from the semiclassical model, with $|P_z| < 1.5$ a.u., the interference patterns are still clear. However, when $|P_z| > 1.5$ a.u., the interference patterns from different rescattering cores will overlap. It is also illustrated in Fig. 3(c) from the TDSE. The interference stripes are well resolved with $|P_z| < 1.5$ a.u., and agree

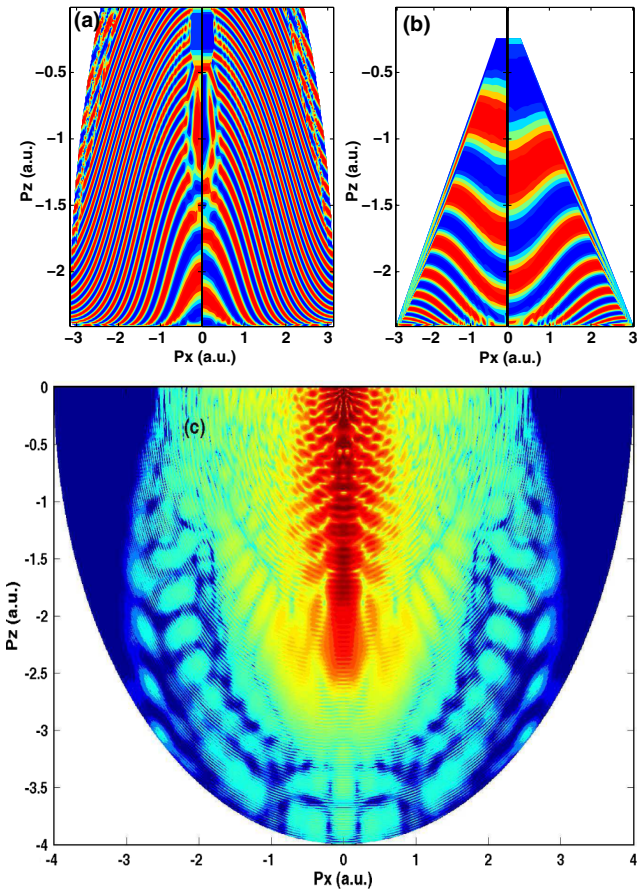

FIG. 3 (color online). The same as Fig. 2, but the molecular axis is parallel to the laser polarization z axis.

well with the semiclassical model presented in Fig. 3(a). The interference structures from short trajectories are difficult to be identified with $|P_z| > 1.5$ a.u. However, for larger transverse momentum, the above additional phase difference is not significant as illustrated in Figs. 3(a) and 3(b), thus allowing us to observe the long trajectory interference channel. Another key point to observe the long trajectory rescattering is to reduce the dispersion of the wave packet. Compared to the perpendicular orientation, the transverse dispersion of the wave packet will be small in parallel orientation due to Coulomb focusing. The long trajectory interference structure is well resolved in the TDSE result in Fig. 3(c) with transverse momentum $|P_x| > 1$ a.u. Although the position of the stripes in Fig. 3(c) does not agree well with the result obtained by the semiclassical model, the width and the space between the stripes from $P_z = -0.5$ to -2.5 a.u. become smaller and smaller, agreeing with the semiclassical model. Taking into account the approximations in the semiclassical model, the predicted backward rescattering APH agree well with the TDSE simulations. The short trajectory PH is well identified both in parallel and perpendicular orientations. However, the observation of the long trajectory APH is optimum in parallel orientation. Since the duration of a laser cycle $T_0 \approx 1.8$ fs, the birth time of each interference stripe in PAD predicted by the semiclassical model is with precision about $\frac{T_0}{100}$, i.e., below 1 a.u. (24 as). Thus we note that APH can record attosecond time-resolved electronic processes.

In summary, we propose a way of dynamic imaging molecular structure by using backward rescattering APH in MATI. The semiclassical model of rescattering in APH has been shown to agree with TDSE simulations, thus offering a physical picture of the new imaging tool. The birth time of reference and signal channels in APH is recorded with attosecond precision. In addition, the spatial information of the molecular structure including orientations and nuclear distance is presented in APH. For parallel orientation, the long trajectory APH is observable readily as compared to perpendicular orientation. The laser parameters used in the current work are experimentally accessible currently. It is hoped that this letter will stimulate experiments.

We thank Dr. S. Chelkowski, K. J. Yuan, and H. Z. Lu for helpful discussions on MATI and also Compute Canada for access to large scale computing facilities.

*Andre.Bandrauk@USherbrooke.ca

[1] D. Gabor, Nature (London) **161**, 777 (1948).
[2] Y. Huismans *et al.*, Science **331**, 61 (2010).
[3] M. Spanner, O. Smirnova, P. B. Corkum, and M. Y. Ivanov, J. Phys. B **37**, L243 (2004).
[4] X. B. Bian, Y. Huismans, O. Smirnova, K. J. Yuan, M. J. J. Vrakking, and A. D. Bandrauk, Phys. Rev. A **84**, 043420 (2011).
[5] P. B. Corkum, Phys. Rev. Lett. **71**, 1994 (1993).
[6] A. D. Bandrauk, S. Chelkowski, and S. Goudreau, J. Mod. Opt. **52**, 411 (2005).
[7] F. Krausz and M. Ivanov, Rev. Mod. Phys. **81**, 163 (2009).
[8] F. Mauger, C. Chandre, and T. Uzer, Phys. Rev. Lett. **104**, 043005 (2010).
[9] T. Zuo, A. D. Bandrauk, and P. B. Corkum, Chem. Phys. Lett. **259**, 313 (1996).
[10] A. D. Bandrauk and M. Ivanov, *Quantum Dynamic Imaging* (Springer, New York, 2011).
[11] H. C. Shao and A. F. Starace, Phys. Rev. Lett. **105**, 263201 (2010).
[12] M. Busuladžić, A. Gazibegović-Busuladžić, D. B. Milošević, and W. Becker, Phys. Rev. Lett. **100**, 203003 (2008).
[13] N. Takemoto and A. Becker, Phys. Rev. Lett. **105**, 203004 (2010).
[14] G. G. Paulus, W. Becker, W. Nicklich, and H. Walther, J. Phys. B **27**, L703 (1994).
[15] M. Lein, J. P. Marangos, and P. L. Knight, Phys. Rev. A **66**, 051404 (2002).
[16] S. Selstø, M. Førre, J. P. Hansen, and L. B. Madsen, Phys. Rev. Lett. **95**, 093002 (2005).
[17] T. Marchenko, Y. Huismans, K. J. Schafer, and M. J. J. Vrakking, Phys. Rev. A **84**, 053427 (2011).